MOL #87833

A single glycine in extracellular loop 1 is the critical determinant for pharmacological

specificity of dopamine D2 and D3 receptors

Mayako Michino, Prashant Donthamsetti, Thijs Beuming, Ashwini Banala, Lihua Duan,

Thomas Roux, Yang Han, Eric Trinquet, Amy Hauck Newman, Jonathan A. Javitch, Lei Shi

Department of Physiology and Biophysics and Institute for Computational Biomedicine, Weill

Medical College of Cornell University, New York, New York (M.M., L.S.); Departments of

Psychiatry and Pharmacology, Columbia University College of Physicians and Surgeons, and

Division of Molecular Therapeutics, New York State Psychiatric Institute, New York, New York

(P.D., L.D., Y.H., J.A.J.); Schrödinger Inc., New York, New York (T.B.); Medicinal Chemistry

Section, Molecular Targets and Medications Discovery Branch, National Institute on Drug Abuse

- Intramural Research Program, Baltimore, Maryland (A.B., A.H.N.); Cisbio Bioassays, Codolet,

France (T.R., E.T.).

Running Title: A single Gly is critical for the specificity of D2R and D3R

Address correspondence to:

Dr. Lei Shi, 1300 York Avenue, Box 75, Weill Cornell Medical College, New York, NY 10065.

Email: les2007@med.cornell.edu

Dr. Jonathan A. Javitch, 1051 Riverside Drive, Unit 19, New York State Psychiatric Institute,

New York, New York 10032, Email: jaj2@columbia.edu

Number of text pages: 21

Number of tables: 2

Number of figures: 7

Number of references: 45

Number of words in the Abstract: 223

Number of words in the Introduction: 566

Number of words in the Discussion: 1485

Abbreviations:

β_1AR, β_1-adrenergic receptor; β_2AR, β_2-adrenergic receptor; D2R, dopamine D2 receptor;

D3R, dopamine D3 receptor; EL1, extracellular loop 1; EL2, extracellular loop 2; FRET,

fluorescence resonance energy transfer; GPCR, G-protein-coupled receptor; HTRF,

Homogeneous Time Resolved FRET; IFD, induced-fit docking; MD, molecular dynamics; MM-

GBSA, molecular mechanics-generalized Born surface area; NAPS, N-

azidophenethylspiperone; OBS, orthosteric binding site; PP, primary pharmacophore; Prokink,

proline kink; REMD, replica exchange MD; RMSD, root-mean-square deviation; SBP, secondary

binding pocket; SP, secondary pharmacophore; SAR, structure-activity relationship; TM,

transmembrane.

Abstract

Subtype-selective agents for the dopamine D3 receptor (D3R) have been considered as potential medications for drug addiction and other neuropsychiatric disorders. Medicinal chemistry efforts have led to the discovery of 4-phenylpiperazine derivatives that are >100-fold selective for D3R over D2R, despite high sequence identity (78% in the transmembrane domain). Based on the recent crystal structure of D3R, we demonstrated that the 4-phenylpiperazine moiety in this class of D3R-selective compounds binds to the conserved orthosteric binding site whereas the extended aryl amide moiety is oriented towards a divergent secondary binding pocket (SBP). In an effort to further characterize molecular determinants of the selectivity of these compounds, we have modeled their binding modes in D3R and D2R by comparative ligand docking and molecular dynamics (MD) simulations. We found that the aryl amide moiety in the SBP differentially induces conformational changes in TM2 and EL1, which amplify the divergence of the SBP in D3R and D2R. Receptor chimera and site-directed mutagenesis studies were used to validate these binding modes and to identify a divergent glycine in EL1 as critical to D3R over D2R subtype-selectivity. A better understanding of drug-dependent receptor conformations such as these is key to the rational design of compounds targeting a specific receptor among closely related homologs, and may also lead to discovery of novel chemotypes that exploit subtle differences in protein conformations.

Introduction

Dopamine receptors, which belong to the class A rhodopsin-like G protein-coupled receptors (GPCRs), are implicated in cognition, motivation, and movement. The dopamine D3 receptor (D3R), a member of the dopamine D2-like receptor subfamily, is a potential therapeutic target for drug abuse and other neuropsychiatric disorders (Heidbreder and Newman, 2010; Newman et al., 2012b). Developing potent and selective D3R ligands is critical to understanding and dissecting its downstream signaling pathways and functional specificity (Holmes et al., 2004). However, the high degree of sequence identity within the transmembrane (TM) domain of D3R and D2R and the near-identity of the orthosteric binding site (OBS) residues, as revealed by the crystal structure of the human D3R (Chien et al., 2010), have made it challenging to create subtype-selective agents, especially with physicochemical properties suitable for *in vivo* characterization of the physiological roles of these receptors.

Notwithstanding these challenges, extensive medicinal chemistry efforts have led to the discovery of a class of 4-phenylpiperazine derivatives that is highly selective for D3R over D2R (e.g. compound R-22 has >100-fold selectivity for D3R over D2R) (Boeckler and Gmeiner, 2006; Newman et al., 2009). These D3R-selective compounds are characterized by a 4-phenylpiperazine primary pharmacophore (PP) and an extended aryl amide secondary pharmacophore (SP) connected by a four-carbon linking chain (Heidbreder and Newman, 2010). Previous structure-activity relationship (SAR) studies have attributed the subtype-selectivity for D3R over D2R to the substituents on the 4-phenylpiperazine, an extended aryl amide ring system, and the length and functionalization of the linking chain (Banala et al., 2011; Grundt et al., 2007; Newman et al., 2009). Based on the crystal structure of D3R, we recently demonstrated that D3R over D2R selectivity mainly arises from divergent interactions of the SP within a second binding pocket (SBP) lined by residues from TMs1, 2, 3, 7, EL1 and EL2 (Newman et al., 2012a).

To date, very limited conformational differences have been observed within the OBS among crystal structures of the same receptor bound to a variety of ligands in the absence of G protein, e.g., the side chain RMSDs of the OBS residues are within 1.0 Å among the crystal structures of β_1-adrenergic receptor (β_1AR) (Katritch et al., 2012). In contrast to this similarity in the OBS, among the β_1AR structures, greater conformational rearrangements are present in regions distal to the OBS when extended or bitopic ligands are bound (Warne et al., 2012; Warne et al., 2011). Interestingly, the SP in the 4-phenylpiperazine class of D3R-selective compounds, an extended aryl amide or bioisostere thereof, interacts with the divergent SBP, the size, shape, and plasticity of which are likely involved in D3R over D2R selectivity. In particular, the conserved flexible proline kinks (Prokinks) in TM2 and TM7 (Ballesteros et al., 2001; Sansom and Weinstein, 2000), together with the divergent EL1, EL2, and extracellular portion of TM1, may allow the SBP of D3R and D2R to adopt different configurations that differentially accommodate the SP of R-22 and other D3R-selective ligands.

To further dissect the structural basis of D3R over D2R selectivity, we carried out comparative computational docking and MD simulations of D3R and D2R models complexed with a variety of 4-phenylpiperazine derivatives, focusing on their access to and binding within the SBP. Combining these data with those from receptor chimera and site-directed mutagenesis studies, we identified a critical receptor segment and then a specific residue in the SBP that are responsible for D3R over D2R selectivity.

Materials and Methods

Ligand preparation and molecular docking

Ligands were docked to an equilibrated model of the D3R crystal structure (PDB ID: 3PBL), and an equilibrated homology model of D2R based on the D3R structure (Chien et al., 2010) by a core-restrained induced-fit docking (IFD) protocol (Newman et al., 2012a; Sherman et al., 2006). The ensemble of IFD poses was clustered by interaction fingerprint analysis with the SIFt module in Maestro (version 9.3; Schrödinger, LLC: New York, NY, 2012), and several representative poses were selected from the largest low-energy clusters. The MM-GBSA receptor-ligand energy was calculated using Prime (version 3.1; Schrödinger, LLC: New York, NY, 2012).

For the MD and REMD simulations, partial charges of the ligand atoms were calculated by the quantum mechanics-polarized ligand docking (QPLD) protocol (Cho et al., 2005) (Schrödinger Suite 2012).

Molecular dynamics

Representative models obtained from the IFD docking trials were re-inserted into the explicit water-membrane bilayer solvent environment, and isothermal-isobaric molecular dynamics (MD) simulations were performed at 310K for 18 ns or longer using Desmond (Desmond Molecular Dynamics System, D. E. Shaw Research, New York, NY, 2012. Maestro-Desmond Interoperability Tools, Schrödinger, New York, NY, 2012). The simulations were carried out until both the receptor and ligand conformations are equilibrated (RMSD to within 1.0 Å for Cα atoms of ligand-interacting residues, and 0.5 Å for the ligand over the last 6 ns of the trajectory). Multiple trajectories were collected for each receptor-ligand complex.

Replica exchange MD (REMD)

REMD enhances conformational sampling by simulating multiple copies (replicas) of the same system at different temperatures and allowing exchanges of replicas between neighboring

temperatures according to the Metropolis criterion (Sugita and Okamoto, 1999), and has been

used in sampling the folding landscape to study protein folding mechanisms (Felts et al., 2004;

Zhou et al., 2001) and predicting protein-ligand interactions (Osguthorpe et al., 2012). REMD

simulations in this study were started from initial configurations with poses different from the

preferred pose as well as from the preferred pose, to demonstrate that a converged equilibrium

distribution of poses can be obtained from different initial configurations. 14 or 18 replicas in the

temperature range of 310 to 333 K were used. The temperature increments, with smaller

spacing at lower temperatures (e.g., from $\Delta T_{1,2}$ = 1.2 to $\Delta T_{17,18}$ = 1.6 in the 18-replica runs),

were chosen to ensure homogeneous acceptance ratio between all temperature pairs over the

entire temperature range (Patriksson and van der Spoel, 2008). The acceptance ratio was

~0.15-0.25. The exchange between replicas was attempted every 1.2 ps, and the simulations

were run for at least 4.5 and up to ~13 ns. During the REMD simulation, most replicas visited

temperatures broadly across the entire range, indicating that the temperature series is

sufficiently optimized and the length of simulation is sufficiently long. Conformations sampled at

each temperature in REMD, like an individual constant temperature MD trajectory, follow a

Boltzmann distribution (Sugita and Okamoto, 1999). Conformational ensembles from the same

statistical distribution can be compared in terms of populations of low-energy conformational

states.

The REMD was performed using Desmond, with all other parameters set to the same values

as in the regular MD. The frames from the last 0.96 ns of the 310 K ensembles were clustered

based on ligand heavy-atom RMSD with a fixed cluster radius of 1.5 Å, using the cluster.pl utility

in MMTSB Tool Set (Feig et al., 2004).

WaterMap calculations

Representative frames were selected from MD ensembles of D3R and D2R stabilized by

ligands R-22 and the C3 analog. For each receptor-ligand complex, a total of 750 frames were

pooled from the last 6-9 ns of several trajectories, and clustered by Cα atoms of extracellular

segments of TMs 2 and 3 (residues 2.58-2.66 and 3.22-3.31) at a fixed cluster radius of 1.5 Å

RMSD, after aligning by Cα atoms of intracellular segments of TMs 2 and 3 (residues 2.38-2.55

and 3.34-3.55). For each cluster, the frame closest to the centroid was included in the

representative set. WaterMap calculations (Abel et al., 2008) were performed on the

representative set.

Conformational analyses

We computed the helix angles of Prokinks at $Pro^{2.59}$ (Pro84 in D3R, Pro89 in D2R) using the

Prokink program in Simulaid (Visiers et al., 2000), which quantifies the kink angle in terms of

three aspects, bend angle, wobble angle, and face shift. We use 7 residues before and after the

proline residue to define the helical segments preceding and following the kink.

We counted the number of water molecules in the SBP to approximate the volume not

occupied by ligand in the SBP. We arbitrarily define a water molecule to be in the SBP if its

oxygen atom is within 5 Å of residues in TMs 1, 2, 3, 7, and EL2 that face the SBP, but not

within 6 Å of lipid atoms, and its z-coordinate is within 12 Å and above that of the $Asp^{3.32}$ Cα

atom (the z-axis is perpendicular to the membrane and points toward the extracellular side).

The flexibility of the receptor-bound ligand conformations was quantified by measuring the

angle formed between the PP and the SP moieties. The angle was obtained using the

fit_angle.py utility in VMD, which measures the angle between the 'best-fit' lines through two

selections. The 'best-fit' line was estimated by a least-squares linear regression model of the

coordinates of the selected atoms.

Receptor chimera creation and site-directed mutagenesis

Wild-type human D3R and D2R were tagged with a signal peptide (Guo et al., 2003)

followed by a hemagglutinin (HA) epitope and SNAP-tag, and cloned into pcDNA5/FRT/TO

(Invitrogen) using standard molecular biology procedures. Chimeric receptors were generated

starting with constructs provided by Robert Luedtke (University of North Texas Health Science Center) (Banala et al., 2011). The NT-TM1-IL1 (residues 1-67), EL1 (residues 98-102), and EL2 (residues 173-185) of D2R alone or in combination were replaced with that of D3R (residues 1-62, 93-98, and 171-184, respectively). Site directed mutants of D3R and D2R were generated using a PCR-based based strategy (QuickChange Site directed mutagenesis, Agilent). All the constructs were confirmed by sequencing analysis.

Radioligand competition and Homogeneous Time Resolved FRET binding

Radioligand binding and HTRF experiments were performed in HEK293 cells stably transfected with SNAP-tagged wildtype or chimeric and mutant receptors using the Flp-in T-Rex system (Invitrogen) and maintained in growth medium (DMEM; 10% FBS; 2 mM L-glutamine). For radioligand competition binding, studies were carried out with 100 pM [^{3}H]N-methylspiperone (PerkinElmer Life Sciences) using 1 µM haloperidol to define nonspecific binding. Cells were induced for 24 hours prior competition binding assay with 1 µg/mL tetracycline. Binding was performed on membrane or whole cell preparations as described previously (Javitch et al., 1995).

For HTRF experiments, 50,000 cells per well were seeded into black 96-well plates (Greiner 655086) pretreated with 50 µg/mL Poly-D lysine. Cells were induced with 1 µg/mL tetracycline in growth medium 24 hours after seeding. 48 hours after seeding, cells were incubated with 100 nM Tag-Lite Lumi4 in growth medium for 1 hour and washed 3 times with Tris-Krebs buffer (20 mM Tris, pH 7.4; 118 mM NaCl; 1.2 mM KH$_2$PO$_4$; 1.2 mM MgSO$_4$; 4.7 mM KCl; 1.8 mM CaCl$_2$). 10 nM of NAPS-DY-647 (Cisbio) along with various concentrations of test ligand in a total volume of 100 µl of Tris-Krebs/0.1% BSA buffer were added to each well and plates were incubated overnight at 4 °C. Preparations were excited at 337 nm (excitation of Tag-Lite Lumi4) and emission was measured at 620 (emission for Tag-Lite Lumi4) and 665 (emission for DY-647) on a Pherastar FS plate reader (BMG Labtechnologies). 400-µs readings were measured

9

after a 50-µs delay to avoid short-life fluorescence background from the signal. Of note, the conditions we used here led to ligand depletion. Additional analysis suggests that lowering the seeded cell number to 10,000 and increasing the volume to 200 µl prevents ligand depletion in the competition assay.

Disintegrations per minute (DPM) from radioligand binding or FRET ratios (665 nm/620 nm) from HTRF competition binding experiments were modeled using nonlinear regression analysis with GraphPad Prism 5 to determine IC_{50} values for each ligand, which were converted to equilibrium dissociation constants (K_i) using the Cheng–Prusoff correction (Cheng and Prusoff, 1973) for radioligand binding data and, to account for ligand depletion, the Munson-Rodbard correction (Munson and Rodbard, 1988) for HTRF binding data. Mean K_i values ± S.E.M. are reported for at least three independent experiments. One-way ANOVA and Bonferonni post-hoc statistical tests were applied using GraphPad Prism 5.

Results

The impact of the linker on D3R over D2R selectivity

Based on molecular docking and dynamics simulations, we previously characterized the

binding mode of compound R-22 in D3R and showed that the SP interacts with a sub-pocket of

the SBP at the interface of TM2, TM3, EL1, and EL2 (Ptm23), formed by residues Val86$^{2.61}$,

Leu89$^{2.64}$, Gly94^{EL1}, Phe106$^{3.28}$, and Cys181^{EL2}. In contrast, in D2R the SP is positioned closer

to the interface of TMs 1, 2, and 7 (Ptm27) and the binding pose is less well-defined (Newman

et al., 2012a).

To further characterize the propensity of the SP indole moiety of R-22 to interact with either

the Ptm23 or Ptm27 sub-pocket of D3R and D2R, we first measured the binding affinities of a

series of R-22 analogs without the 3-OH group and with either 3, 4, or 5 carbon atoms in the

linking chain (C3, C4, and C5, respectively; the C4 analog was previously described (Newman

et al., 2012a); synthesis of the C3 and C5 analogs is described in the Supplemental Data). As

seen with a previously reported set of 2,3-diCl-phenylpiperazine analogs (Robarge et al., 2001),

the C4 analog is the most D3R selective (~46-fold), whereas the C3 analog has significantly

lower affinity for D3R compared to R-22 and the C4 analog, resulting in a nearly complete loss

of selectivity for D3R over D2R (Fig. 1, Table 1). The C5 analog retains high affinity for D3R,

albeit ~5-fold lower than the C4 analog, and has slightly improved affinity for D2R, resulting in

only ~9-fold selectivity for D3R. We hypothesized that the shorter linker in the C3 analog

prevents the optimal placement of the SP in the Ptm23 sub-pocket of D3R, leading to the

observed changes in binding affinity.

To explore this hypothesis, we carried out molecular dynamics (MD) simulations of models

of D3R or D2R complexed with R-22, as well as the C3, C4, and C5 analogs (Fig. 2). To reduce

bias due to the choice of starting conformation, multiple MD simulations (~20 ns each) were

started from representative docked poses that positioned the SP in different sub-pockets within

the SBP (Supplemental Table 1). The SP behaved differently in D3R and D2R: in 5 of the 6

D3R/R-22 trajectories, the SP interacted with the Ptm23 sub-pocket, while in all D2R/R-22

trajectories, the SP interacted with the Ptm27 sub-pocket (Supplemental Fig. 1). When we

forced the SP into Ptm23 of D2R by docking, this resulted in binding poses characterized by a

highly strained linker region (data not shown). Similar to the results for R-22, the analysis of C4

analog trajectories showed a tendency for its SP to interact with the Ptm23 sub-pocket in D3R,

and with the Ptm27 sub-pocket in D2R (Supplemental Table 1). Of note, the SP poses for C4

were more broadly distributed compared to that of R-22 in D2R (larger standard deviations for

the angle between the axes of the PP and the SP moieties, 124.9 ± 8.7 degrees for R-22, and

121.3 ± 11.2 degrees for C4). A similar trend was also observed in D3R but to a lesser extent

(132.5 ± 5.4 degrees for R-22 and 129.4 ± 7.4 degrees for C4). The narrower distribution of SP

poses for R-22 may result from the H-bond formed between the 3-OH in the linker and Tyr[7.43].

In the D3R/C3 analog simulations, we found that the indole ring of the SP tended to be

perpendicular to the Ptm23 sub-pocket (defined as Ptm23' in Supplemental Table 1; see

Supplemental Fig. 2), where it is not as tightly packed against the Ptm23 residues as is the case

for R-22 (Supplemental Fig. 1). In D2R/C3 analog simulations, the SP was either in the Ptm23'

pose or extensively exposed to the water phase (Supplemental Table 1).

We sought to improve sampling further by carrying out replica exchange molecular

dynamics (REMD) simulations. REMD is an advanced sampling technique that enhances

conformational sampling compared to regular constant-temperature MD (Sugita and Okamoto,

1999) (see Methods), and has been used previously to optimize sampling of protein-ligand

binding modes (Osguthorpe et al., 2012). As expected, the 310 K REMD ensembles (enhanced

by the exchange of states sampled at higher temperatures) show better convergence of ligand

binding poses compared to the corresponding regular MD ensembles generated at 310 K (see

Supplemental Tables 1 and 2, Supplemental Fig. 3). Specifically, in the REMD simulations of

the D3R and D2R in complex with R-22 starting with the SP of R-22 interacting with Ptm27

(Supplemental Table 2), the analysis of the 310 K ensembles showed that the R-22 in D3R

gradually became more populated with poses having the SP in the Ptm23 sub-pocket, while the

SP in the D2R simulations remained in the Ptm27 sub-pocket. Thus, our REMD results are

consistent with the results from regular MD, suggesting distinct binding modes of R-22 in D3R

and D2R (Fig. 2A, B and C). In the REMD simulations of the D3R/C3 analog complex starting

from binding poses in which the SP was positioned close to Ptm23, we found that the 310 K

ensembles tend to be populated with the SP moiety adopting the alternate pose Ptm23',

consistent with the MD results. In this pose, the SP moiety loses contacts with two residues of

Ptm23, Gly94 and Val86$^{2.61}$ (Fig. 2F, Supplemental Fig. 1C). Thus the shorter linker results in

the SP being positioned further from Gly94 in EL1 than is the case for R-22 (Fig. 3,

Supplemental Table 3). When the REMD simulations of the D2R/C3 analog complex were

started from poses in which the SP interacted with either Ptm23 or Ptm27, the resulting 310 K

ensembles consisted of a spectrum of poses that are not in tight association with either of the

Ptm23 and Ptm27 sub-pockets (Fig. 2G). These simulations show that the SP moiety of the C3

analog does not associate tightly with the Ptm23 sub-pocket in either D3R or D2R, consistent

with the lower binding affinity for D3R compared to R-22 and the C4 analog. By contrast, MD

and REMD simulations of the C5 analog with D3R and D2R show that the SP moiety interacts

preferably with Ptm23 in D3R but is positioned further away from the pocket in D2R, consistent

with its higher affinity for D3R.

Divergence in the size and shape of the SBP in D3R and D2R

Using comparative MD simulations with the D3R and D2R models complexed with the non-

selective ligand eticlopride, we showed previously that the orientation of the SBP with respect to

the highly conserved OBS is divergent in D3R and D2R (Chien et al., 2010). The difference in

distance between two conserved residues, Glu$^{2.65}$ (in the SBP) and Tyr$^{7.43}$ (at the border of the

13

SBP and OBS), can be as large as 2 Å between D3R and D2R despite the fact that eticlopride, unlike R-22, does not substantially occupy the SBP (Chien et al., 2010). This suggests that the volume of the SBP in the D3R and D2R is likely to be different. To characterize this volume, we counted the number of water molecules in the SBP during MD simulations (as the number of waters correlates with volume under constant temperature and constant pressure MD simulation conditions). We found a significantly greater number of waters in D3R than in D2R in the eticlopride-bound MD simulations, supporting an intrinsic divergence of this region in the two receptors. In addition, water counts in frames collected from MD trajectories of D3R and D2R complexed with R-22 were also significantly greater in D3R compared to D2R ($p < 0.0005$), suggesting that the volume of the SBP remains larger in D3R than in D2R even when a sub-pocket of SBP is occupied (Supplemental Fig. 4).

To identify differences between D3R and D2R not only in size but also in the shape of the SBP, we analyzed and compared the receptor conformations around the SBP from MD trajectories of D3R and D2R complexed with R-22 or its C4 analog. For both compounds, we observed conformational rearrangements of the SBP with respect to the eticlopride-bound state in D3R but not in D2R. We quantified these differences with Prokink angle measurements (Shi et al., 2001; Visiers et al., 2000) at the conserved Pro[2.59]. The results showed that wobble angles in the D3R models complexed with these two compounds are ~15 degrees greater than in the D3R models complexed with eticlopride, corresponding to an outward rearrangement of the extracellular segment of TM2 (Fig. 4). In contrast, no significant changes were observed in D2R bound to the two ligands. This trend correlates with the SP binding to the Ptm23 in D3R and the Ptm27 in D2R (Supplemental Table 4; Fig. 2A). Interestingly, the models bound to 4-phenylpiperazine synthons BEN 01-30 and BAK 02-43 that do not contain a SP (Newman et al., 2012a) and do not reach the Ptm23 sub-pocket have Prokink angles similar to those in the eticlopride-bound conformations, suggesting that the conformational change is dependent upon

14

the presence of the SP in the Ptm23 sub-pocket (Supplemental Table 4). In the case of the C3

analog, the Prokink angles do not differ significantly from the eticlopride-bound conformations in

either D3R or D2R, which is again consistent with relatively weak interactions between the SP

and Ptm23, as discussed above.

To assess whether the structural divergence between D2R and D3R in the induced-

conformations of the SBP results in a general difference in the capacity for binding small-

molecules, we characterized the SBP using WaterMap calculations. WaterMap describes the

thermodynamic properties of hydration sites in ligand binding pockets. The displacement of

hydration sites with high free energy contributes favorably to the affinity of a ligand. Recent

benchmark studies have documented the ability of this method to distinguish binding sites of low

and high affinities (Beuming et al., 2012; Mason et al., 2012). When the D3R-Ptm23 sub-pocket

is occupied by R-22, a cluster of three high-energy hydration sites is displaced by the indole

ring, consistent with the high affinity of Ptm23-bound R-22 in D3R (see large spheres in Fig.

5A). This displacement of high-energy sites is not observed in the C3 analog bound D3R

conformation (Fig. 5C). In the R-22-bound D2R conformation, the Ptm27 sub-pocket contains

hydration sites of significantly lower energy, thereby limiting the contribution of solvent

displacement on the affinity of the ligand (Fig. 5B). For the C3-bound D2R conformation, not

only is the pose less tightly associated with Ptm23 (as revealed by a large distance (> ~8 Å)

between the SP and Gly98 in EL1) but the sub-pocket also contains fewer high energy sites

than Ptm23 in the R-22-bound D3R conformation (Fig. 5D). In summary, only the R-22 bound

D3R model is consistent with a substantial displacement of high energy hydration sites from the

receptor by the bound ligand, in agreement with the observed high affinity of this ligand/receptor

complex.

EL1 is critical for D3R over D2R selectivity

Based on these computational results, we hypothesized that the ability of the SP to adopt a favorable binding pose in Ptm23 is dependent on local conformational flexibility. In particular, the flexibility of TM2 is likely determined both by the conserved Pro$^{2.59}$, which acts as a hinge, and by the length and configuration of EL1, which modulates the degree of bending at the Prokink (Fig. 4A). EL1 in D3R is one residue longer than in D2R: D3R has two Gly residues in EL1 (93GGV95), whereas D2R has only one Gly residue (98GE99). Whereas Gly94 in D3R faces Ptm23, in D2R the structurally aligned Gly98 does not directly face Ptm23 (Supplemental Fig. 5). Differences in the electrostatic properties near Ptm23 may also contribute to the D3R over D2R selectivity of R-22 and related compounds, and there are two negatively charged residues, Glu99 and Glu181, in EL1 and EL2, respectively, that are present in D2R, but not D3R (Chien et al., 2010) (Supplemental Fig. 5).

To test our hypothesis that the Prokink in TM2 and EL1 play an important role in selectivity, we carried out binding experiments on mutants of D3R and D2R lacking the TM2 Prokink, as well as D3R/D2R receptor chimeras in which the extracellular segments of D2R, including the N-terminus-TM1-IL1, EL1, EL2 alone or in combination were swapped with that of D3R (Fig. 6A, Table 2). In order to screen a large number of mutants and chimeras efficiently, we used a homogeneous time-resolved FRET (HTRF)-based binding assay (Albizu et al., 2010) to determine affinities of the non-selective D2R-like sub-family ligand NAPS as well as R-22. Receptors were N-terminally tagged with a SNAP tag, which can be covalently labeled using a benzyl guanine terbium-based donor chromophore. When a NAPS-DY-647 acceptor chromophore is bound to the OBS of the receptor, there is a detectable FRET signal that can be used to quantitate competition by an unlabeled ligand (Fig. 6B).

To probe the role of the TM2 Prokink in selectivity, Pro$^{2.59}$ was mutated to alanine in both the D2R and D3R. Unfortunately, specific binding to these mutants was too low to determine

16

binding affinities of NAPS or R-22 in the intact cell HTRF assay as well as in the radioligand

binding assay with membrane preparations. Efforts to enhance expression or folding using

possible chaperones, including the membrane permeant receptor antagonist raclopride and

DMSO as well as prolonged incubation of cells at temperatures shown to overcome folding

abnormalities in other GPCRs (Segaloff, 2012) failed to enhance binding (data not shown),

highlighting the importance of this conserved Pro for proper receptor folding.

In contrast, chimeric receptors used to probe the role of NT-TM1-IL1, EL1 and EL2 in R-22

selectivity were properly folded based on the finding that NAPS affinity was not significantly

affected by exchange of any receptor segment tested (Table 2). However, swapping the EL1 of

D3R but not the N-terminus-TM1-IL1 or EL2 segment alone into D2R resulted in a ~12-fold

increase in the affinity of R-22, consistent with our prediction that EL1 is the critical structural

determinant of D3R-selectivity (Fig. 6C). Consistent with this finding, R-22 affinity was enhanced

significantly in all D2R chimeras containing EL1 from D3R (Table 2).

A critical role for an EL1 glycine in determining D3R over D2R selectivity

Strikingly, upon further dissection of EL1, we found that the impact of swapping EL1 can be

attributed to a single Gly residue. Remarkably, the insertion of an extra Gly residue at position

98 in D2R (D2RGGE) increased R22's affinity ~16 fold to the same level as swapping EL1, not

significantly different from that of D3R, whereas deletion of Gly94 in D3R (D3RΔ94G) lowered

affinity ~24-fold, essentially to that of D2R (Fig. 6D). In contrast, removal of the negative

charges in EL1 and EL2 (E99V or E181V) had no impact on R-22 affinity in D2R (Fig. 6E).

Curiously, the extent of R-22 selectivity for D3R over D2R was slightly less when measured

in the HTRF assay (~48 fold) than in the radioligand binding assay (~157 fold). To confirm that

the determinants of selectivity were similar in both assays we reassayed the selectivity of NAPS

and R-22 for selected chimeras and point mutants in the radioligand membrane binding assay

and validated our findings regarding their critical contribution to the pharmacological specificity

of R-22 (Supplemental Table 5).

Of note, our HTRF assay used intact cells, whereas radioligand binding used a membrane

preparation. Surprisingly, when we carried out radioligand binding assays with intact cells, the

selectivity measurements were more similar to that of the HTRF results (Supplemental Table 6).

In both intact cell assays the affinity of R-22 for the D3R is several-fold lower than in

membranes, which leads to several-fold lower selectivity ratios. Thus, it is the receptor

preparation and not the probe or assay format that contributes to the observed selectivity

differences. The explanation for this difference is unclear and merits further study and attention

in comparing results from different assays.

18

Discussion

Our simulations of D3R and D2R in complex with D3R-selective 4-phenylpiperazine compounds suggest that the extra Gly94 in EL1 modulates specificity for D3R in multiple ways: i) it interacts directly with the SP of R-22, and ii) it gives EL1 sufficient flexibility to allow the outward conformational rearrangement of TM2 necessary for the Ptm23 sub-pocket to accommodate optimally the SP of R-22. This is consistent with the dramatic loss of affinity of R-22 for D3R when this residue is deleted, and the large increase of affinity of R-22 for D2R when a Gly is inserted into EL1. In addition, computational hydration site predictions suggest that the Ptm23 sub-pocket has higher binding affinity in D3R than in D2R, which is optimally exploited by the R-22 binding mode in the SBP. Thus, our combined computational and experimental results point to the difference in the conformations of the SBP between D3R and D2R and identify TM2 and EL1 as the critical determinants for D3R over D2R selectivity. Interestingly, TM2 plays a critical role in selectivity despite being completely conserved between the two receptors. This is due to an alteration of its positioning as a result of the additional Gly, which lengthens EL1 and allows TM2 to move.

Comparison of the available inactive structures of the β_1AR (11 structures, PDB IDs: 2VT4, 2Y00, 2Y01, 2Y04, 2Y02, 2Y03, 2YCW, 2YCX, 2YCZ, 4AMI, 4AMJ) vs. the β_2AR (6 structures, PDB IDs: 2RH1, 3D4S, 3NY8, 3NY9, 3NYA, 3PDS) shows a remarkable parallel to our findings for the specificity determinants of R-22 for D3R over D2R. Thus, the extent of structural rearrangements of EL1 and TM2 induced by bulky ligands is correlated with the presence of a Gly residue in EL1 of β_1AR but not β_2AR. In β_1AR, the bulky ligand carvedilol induces an outward shift of the extracellular segment of TM2 (PDB ID: 4AMJ (Warne et al., 2012)), resulting in 2.3 Å outward movement of the Cα atom of Gly105 compared to the receptor complexed with the smaller ligand cyanopindolol (PDB ID: 2VT4 (Warne et al., 2008))(Fig. 7A). In contrast, in β_2AR, the bulky ligand, FAUC50 (PDB ID: 3PDS (Rosenbaum et al., 2011)), does not induce

any outward shift of TM2 (Fig. 7B). Thus, the presence of Gly105 in EL1 of β_1AR and the lack of a Gly residue at the aligned position in EL1 of β_2AR likely contributes to the difference in the flexibility of the extracellular portion of the TM2 Prokink between β_1AR and β_2AR, in a manner highly analogous to that observed in D3R and D2R. Similarly, modeling studies of the A_3 adenosine receptor in complex with an agonist containing rigid C2 extensions have suggested that an outward displacement of TM2 is required to accommodate such a bulky ligand (Tosh et al., 2012).

Prior chimeric receptor and mutagenesis studies were consistent with a contribution of a region containing EL1 and, to a much lesser degree, EL2, in D3R over D2R selectivity for R-22 (Newman et al., 2009) and another highly D3R-selective F-analog of R-22 (Banala et al., 2011). The current results detail the specific contribution of EL1 to the D3R over D2R selectivity of R-22 and C4 analog, and identify Gly94 as the critical residue in D3R for this selectivity, through its ability to modulate the size and shape of the SBP and allow the SP to bind in Ptm23. The combination of EL1 and EL2 led to a slightly greater D3R-selectivity (Table 2), consistent with the higher affinity seen for the F-analog of R-22 in the D2R chimera that included both EL1 and EL2 of D3R (Banala et al., 2011). EL2 may act synergistically with EL1, given the extensive interactions in our models between EL1 and EL2 that involve divergent residues in D3R and D2R. In D3R, Val95 and Asn97 of EL1 interact with Val180 and Thr179 of EL2, respectively, while in D2R, the corresponding interactions are formed between charged Glu99 and Lys101 of EL1 and Glu181 and Asn180 of EL2 (Supplemental Fig. 5). Interestingly, the Ptm23 sub-pocket overlaps with the aromatic microdomain in TMs 2, 3, and 7 of D2R that had been identified by mutagenesis experiments to contribute to D4R over D2R selectivity, in this case through steric clash of the bulky substituents on the D4R-selective antagonists with this domain (Simpson et al., 1999).

20

Among β-adrenergic and muscarinic receptor subtypes, poorly conserved regions in the extracellular vestibule of the receptor have been proposed to act as a potential "selectivity filter", influencing association and dissociation kinetics of the ligands as they enter the binding pocket, and it has been suggested that different interactions with the filter between the subtypes might provide opportunities for design of subtype-specific ligands (Dror et al., 2011; Kruse et al., 2012). Similarly, we propose a strategy for designing subtype-selective ligands for highly homologous GPCRs by targeting nonconserved binding pockets adjacent to the OBS by designing bivalent ligands in which the second pharmacophore can optimally access sub-pockets in the SBP. It is important to note that the divergence of these sub-pockets can result either from lack of conservation of component residues or from differences in structural plasticity that stem from differences elsewhere, or both. Indeed, targeting the differential conformational plasticity of a binding site has been proposed as an approach to designing selective ligands (Huggins et al., 2012).

Consistent with our previous results (Newman et al., 2012a), our analysis of the angle between the axes of the PP and the SP moieties quantitatively demonstrated that the SP poses of R-22 and C4 are more widely distributed in D2R compared to their poses in D3R due to the less tight binding in Ptm27 than Ptm23. Such differences in flexibility also provide interesting clues about the entropy contribution to the binding of these ligands. Thus, although the 3-4 fold affinity difference between R22 and C4 at D2R is likely beyond the predictive power of computational modeling, it is possible that configurational entropy differences (Gilson and Zhou, 2007) between the binding poses of R-22 and C4 account for the small differences in their affinities for the D2R – the entropy penalty due to the loss of the flexibility by the constraining effect of the 3-OH on R-22 is larger than the favorable enthalpic contribution to the binding affinity by the H-bond. In comparison, the enthalpy, i.e., the optimal interactions between the SP and Ptm23, is dominant in the R-22 and C4 binding in D3R, which results in similar affinities of

these two compounds in D3R. Interestingly, it has been noted that as the size of a compound increases, especially starting around the size of C4 or R-22 (30 and 31 heavy atoms respectively), entropic contributions become more and more important to binding affinity (Hann and Keseru, 2012).

In the compounds studied here, the length of the linker determines to a large extent whether the SP can optimally access Ptm23. Thus, the C3 analog with one fewer carbon in the linker region loses high affinity for D3R compared to R-22, whereas its affinity for D2R remains weak. Our simulations show that the SP of this analog is less tightly associated with the Ptm23 sub-pocket in D3R (Fig. 2F) than is R-22. We have previously reported that the 3-carbon linked analog of the prototypic D3R selective antagonist, NGB 2904, showed ~100-fold decrease in D3R affinity, but remained D3R selective, as did another 3-carbon linked analog with the 2,3-diCl-substituted 4-phenylpiperazine (Robarge et al., 2001). In contrast, a 2-OCH$_3$-substituted 4-phenylpiperazine derivative with a 3-carbon linker has previously been reported to be ~14-fold selective for D2R over D3R (Ehrlich et al., 2009). The decrease in D3R affinity in this case was also accompanied by an increase in D2R affinity and could be due to the 2-OCH$_3$ substitution of the 4-phenylpiperazine bound in the OBS and/or the azaindole as the SP. Collectively, these findings underscore the nature and influence of the PP in the OBS and the SP in the SBP to D3R selectivity, as we have described previously (Newman et al., 2012a).

Being able to computationally simulate and predict locally induced conformational changes by different ligands based on crystal structures is of great interest not only because of the implications for the design of subtype-selective ligands, but also because these ligand-specific conformations may represent distinct functionally selective states. Schwartz and colleagues have previously suggested the important role of a so-called "minor binding pocket" surrounding the conserved TM2 Prokink in receptor activation and functional selectivity, e.g., in angiotensin AT1 receptor (Rosenkilde et al., 2010) – this pocket is very similar to the SBP described here for

D2R and D3R. Furthermore, Chen et al. have recently shown that the bicyclic aromatic moiety of the aripiprazole scaffold plays a critical role in modulating the functional selectivity of these analogs at the D2R (Chen et al., 2012). The binding mode of the bicyclic aromatic moiety in the SBP and the correspondingly induced receptor conformational changes could well be the structural basis for functional selectivity of these aripiprazole derivatives.

Acknowledgements

Authorship Contributions

Participated in research design: Michino, Donthamsetti, Duan, Newman, Javitch, Shi.

Conducted experiments: Michino, Donthamsetti, Beuming, Banala, Duan, Han, Shi.

Contributed new reagents or analytic tools: Michino, Banala, Roux, Trinquet, Newman, Shi.

Performed data analysis: Michino, Donthamsetti, Beuming, Duan, Han, Shi.

Wrote or contributed to the writing of the manuscript: Michino, Donthamsetti, Beuming, Newman, Javitch, Shi.

References

Abel R, Young T, Farid R, Berne BJ and Friesner RA (2008) Role of the active-site solvent in the thermodynamics of factor Xa ligand binding. *J Am Chem Soc* **130**(9): 2817-2831.

Albizu L, Cottet M, Kralikova M, Stoev S, Seyer R, Brabet I, Roux T, Bazin H, Bourrier E, Lamarque L, Breton C, Rives ML, Newman A, Javitch J, Trinquet E, Manning M, Pin JP, Mouillac B and Durroux T (2010) Time-resolved FRET between GPCR ligands reveals oligomers in native tissues. *Nat Chem Biol* **6**(8): 587-594.

Ballesteros JA, Shi L and Javitch JA (2001) Structural mimicry in G-protein-coupled receptors: implications of the high-resolution structure of rhodopsin for structure-function analysis of rhodopsin-like receptors. *Mol Pharmacol* **60**(1): 1-19.

Banala AK, Levy BA, Khatri SS, Furman CA, Roof RA, Mishra Y, Griffin SA, Sibley DR, Luedtke RR and Newman AH (2011) N-(3-fluoro-4-(4-(2-methoxy or 2,3-dichlorophenyl)piperazine-1-yl)butyl)arylcarboxamides as selective dopamine D3 receptor ligands: critical role of the carboxamide linker for D3 receptor selectivity. *J Med Chem* **54**(10): 3581-3594.

Beuming T, Che Y, Abel R, Kim B, Shanmugasundaram V and Sherman W (2012) Thermodynamic analysis of water molecules at the surface of proteins and applications to binding site prediction and characterization. *Proteins* **80**(3): 871-883.

Beuming T, Farid R and Sherman W (2009) High-energy water sites determine peptide binding affinity and specificity of PDZ domains. *Protein Sci* **18**(8): 1609-1619.

Boeckler F and Gmeiner P (2006) The structural evolution of dopamine D3 receptor ligands: structure-activity relationships and selected neuropharmacological aspects. *Pharmacol Ther* **112**(1): 281-333.

Chen X, Sassano MF, Zheng L, Setola V, Chen M, Bai X, Frye SV, Wetsel WC, Roth BL and Jin J (2012) Structure--functional selectivity relationship studies of beta-arrestin-biased dopamine D(2) receptor agonists. *J Med Chem* **55**(16): 7141-7153.

Cheng Y and Prusoff WH (1973) Relationship between the inhibition constant (K1) and the concentration of inhibitor which causes 50 per cent inhibition (I50) of an enzymatic reaction. *Biochemical pharmacology* **22**(23): 3099-3108.

Chien EY, Liu W, Zhao Q, Katritch V, Han GW, Hanson MA, Shi L, Newman AH, Javitch JA, Cherezov V and Stevens RC (2010) Structure of the human dopamine D3 receptor in complex with a D2/D3 selective antagonist. *Science* **330**(6007): 1091-1095.

Cho AE, Guallar V, Berne BJ and Friesner R (2005) Importance of accurate charges in molecular docking: quantum mechanical/molecular mechanical (QM/MM) approach. *J Comput Chem* **26**(9): 915-931.

Dror RO, Pan AC, Arlow DH, Borhani DW, Maragakis P, Shan Y, Xu H and Shaw DE (2011) Pathway and mechanism of drug binding to G-protein-coupled receptors. *Proc Natl Acad Sci U S A* **108**(32): 13118-13123.

Ehrlich K, Gotz A, Bollinger S, Tschammer N, Bettinetti L, Harterich S, Hubner H, Lanig H and Gmeiner P (2009) Dopamine D2, D3, and D4 selective phenylpiperazines as molecular probes to explore the origins of subtype specific receptor binding. *J Med Chem* **52**(15): 4923-4935.

Feig M, Karanicolas J and Brooks CL, 3rd (2004) MMTSB Tool Set: enhanced sampling and multiscale modeling methods for applications in structural biology. *J Mol Graph Model* **22**(5): 377-395.

Felts AK, Harano Y, Gallicchio E and Levy RM (2004) Free energy surfaces of beta-hairpin and alpha-helical peptides generated by replica exchange molecular dynamics with the AGBNP implicit solvent model. *Proteins* **56**(2): 310-321.

Gilson MK and Zhou HX (2007) Calculation of protein-ligand binding affinities. *Annu Rev Biophys Biomol Struct* **36**: 21-42.

Grundt P, Prevatt KM, Cao J, Taylor M, Floresca CZ, Choi JK, Jenkins BG, Luedtke RR and
Newman AH (2007) Heterocyclic analogues of N-(4-(4-(2,3-dichlorophenyl)piperazin-1-
yl)butyl)arylcarboxamides with functionalized linking chains as novel dopamine D3 receptor
ligands: potential substance abuse therapeutic agents. *J Med Chem* **50**(17): 4135-4146.

Guo W, Shi L and Javitch JA (2003) The fourth transmembrane segment forms the interface of
the dopamine D2 receptor homodimer. *J Biol Chem* **278**(7): 4385-4388.

Hann MM and Keseru GM (2012) Finding the sweet spot: the role of nature and nurture in
medicinal chemistry. *Nat Rev Drug Discov* **11**(5): 355-365.

Heidbreder CA and Newman AH (2010) Current perspectives on selective dopamine D(3)
receptor antagonists as pharmacotherapeutics for addictions and related disorders. *Ann N Y
Acad Sci* **1187**: 4-34.

Holmes A, Lachowicz JE and Sibley DR (2004) Phenotypic analysis of dopamine receptor
knockout mice; recent insights into the functional specificity of dopamine receptor subtypes.
Neuropharmacology **47**(8): 1117-1134.

Huggins DJ, Sherman W and Tidor B (2012) Rational approaches to improving selectivity in
drug design. *J Med Chem* **55**(4): 1424-1444.

Javitch JA, Fu D and Chen J (1995) Residues in the fifth membrane-spanning segment of the
dopamine D2 receptor exposed in the binding-site crevice. *Biochemistry* **34**(50): 16433-
16439.

Katritch V, Cherezov V and Stevens RC (2012) Diversity and modularity of G protein-coupled
receptor structures. *Trends Pharmacol Sci* **33**(1): 17-27.

Kruse AC, Hu J, Pan AC, Arlow DH, Rosenbaum DM, Rosemond E, Green HF, Liu T, Chae PS,
Dror RO, Shaw DE, Weis WI, Wess J and Kobilka BK (2012) Structure and dynamics of the
M3 muscarinic acetylcholine receptor. *Nature* **482**(7386): 552-556.

Mason JS, Bortolato A, Congreve M and Marshall FH (2012) New insights from structural biology into the druggability of G protein-coupled receptors. *Trends Pharmacol Sci* **33**(5): 249-260.

Munson PJ and Rodbard D (1988) An exact correction to the "Cheng-Prusoff" correction. *Journal of receptor research* **8**(1-4): 533-546.

Newman AH, Beuming T, Banala AK, Donthamsetti P, Pongetti K, LaBounty A, Levy B, Cao J, Michino M, Luedtke RR, Javitch JA and Shi L (2012a) Molecular determinants of selectivity and efficacy at the dopamine D3 receptor. *J Med Chem* **55**(15): 6689-6699.

Newman AH, Blaylock BL, Nader MA, Bergman J, Sibley DR and Skolnick P (2012b) Medication discovery for addiction: translating the dopamine D3 receptor hypothesis. *Biochemical pharmacology* **84**(7): 882-890.

Newman AH, Grundt P, Cyriac G, Deschamps JR, Taylor M, Kumar R, Ho D and Luedtke RR (2009) N-(4-(4-(2,3-dichloro- or 2-methoxyphenyl)piperazin-1-yl)butyl)heterobiarylcarboxamides with functionalized linking chains as high affinity and enantioselective D3 receptor antagonists. *J Med Chem* **52**(8): 2559-2570.

Osguthorpe DJ, Sherman W and Hagler AT (2012) Exploring protein flexibility: incorporating structural ensembles from crystal structures and simulation into virtual screening protocols. *J Phys Chem B* **116**(23): 6952-6959.

Patriksson A and van der Spoel D (2008) A temperature predictor for parallel tempering simulations. *Physical Chemistry Chemical Physics* **10**(15): 2073-2077.

Robarge MJ, Husbands SM, Kieltyka A, Brodbeck R, Thurkauf A and Newman AH (2001) Design and synthesis of [(2,3-dichlorophenyl)piperazin-1-yl]alkylfluorenylcarboxamides as novel ligands selective for the dopamine D3 receptor subtype. *J Med Chem* **44**(19): 3175-3186.

Rosenbaum DM, Zhang C, Lyons JA, Holl R, Aragao D, Arlow DH, Rasmussen SG, Choi HJ, Devree BT, Sunahara RK, Chae PS, Gellman SH, Dror RO, Shaw DE, Weis WI, Caffrey M, Gmeiner P and Kobilka BK (2011) Structure and function of an irreversible agonist-beta(2) adrenoceptor complex. *Nature* **469**(7329): 236-240.

Rosenkilde MM, Benned-Jensen T, Frimurer TM and Schwartz TW (2010) The minor binding pocket: a major player in 7TM receptor activation. *Trends Pharmacol Sci* **31**(12): 567-574.

Sansom MS and Weinstein H (2000) Hinges, swivels and switches: the role of prolines in signalling via transmembrane alpha-helices. *Trends Pharmacol Sci* **21**(11): 445-451.

Segaloff DL (2012) Regulatory Processes Governing the Cell Surface Expression of LH and FSH Receptors. *Subcell Biochem* **63**: 113-129.

Sherman W, Day T, Jacobson MP, Friesner RA and Farid R (2006) Novel procedure for modeling ligand/receptor induced fit effects. *J Med Chem* **49**(2): 534-553.

Shi L, Simpson MM, Ballesteros JA and Javitch JA (2001) The first transmembrane segment of the dopamine D2 receptor: accessibility in the binding-site crevice and position in the transmembrane bundle. *Biochemistry* **40**(41): 12339-12348.

Simpson MM, Ballesteros JA, Chiappa V, Chen J, Suehiro M, Hartman DS, Godel T, Snyder LA, Sakmar TP and Javitch JA (1999) Dopamine D4/D2 receptor selectivity is determined by A divergent aromatic microdomain contained within the second, third, and seventh membrane-spanning segments. *Mol Pharmacol* **56**(6): 1116-1126.

Sugita Y and Okamoto Y (1999) Replica-exchange molecular dynamics method for protein folding. *Chemical Physics Letters* **314**(1–2): 141-151.

Tosh DK, Deflorian F, Phan K, Gao ZG, Wan TC, Gizewski E, Auchampach JA and Jacobson KA (2012) Structure-guided design of A(3) adenosine receptor-selective nucleosides: combination of 2-arylethynyl and bicyclo[3.1.0]hexane substitutions. *J Med Chem* **55**(10): 4847-4860.

Visiers I, Braunheim BB and Weinstein H (2000) Prokink: a protocol for numerical evaluation of helix distortions by proline. *Protein Eng* **13**(9): 603-606.

Warne T, Edwards PC, Leslie AG and Tate CG (2012) Crystal Structures of a Stabilized beta(1)-Adrenoceptor Bound to the Biased Agonists Bucindolol and Carvedilol. *Structure* **20**(5): 841-849.

Warne T, Moukhametzianov R, Baker JG, Nehme R, Edwards PC, Leslie AG, Schertler GF and Tate CG (2011) The structural basis for agonist and partial agonist action on a beta(1)-adrenergic receptor. *Nature* **469**(7329): 241-244.

Warne T, Serrano-Vega MJ, Baker JG, Moukhametzianov R, Edwards PC, Henderson R, Leslie AG, Tate CG and Schertler GF (2008) Structure of a beta1-adrenergic G-protein-coupled receptor. *Nature* **454**(7203): 486-491.

Zhou R, Berne BJ and Germain R (2001) The free energy landscape for beta hairpin folding in explicit water. *Proc Natl Acad Sci U S A* **98**(26): 14931-14936.

Footnotes

M.M. and P.D. contributed equally to the work.

Figure Legends

Figure 1. Binding affinity of R-22 and its analogs to D3R and D2R. Radioligand competition binding curves for (**A**) R-22 and non-selective D2R-like family antagonist NAPS and (**B**) R-22 analogs C3, C4, and C5. Binding curves are representatives of at least three independent experiments, for which data are summarized in Table 1.

Figure 2. Binding mode of R-22 and the C4 and C3 analogs in D3R and D2R. **A**) The superimposed binding modes of R-22 in D3R (light gray) and D2R (dark gray). The SP of R-22 (thick and thin sticks in D3R and D2R respectively) interacts with the Ptm23 sub-pocket in D3R, and with the Ptm27 sub-pocket in D2R. For receptor-ligand complexes, R-22 (orange lines in **B** and **C**), C4 (yellow lines in **D** and **E**), or C3 (magenta lines in **F** and **G**) bound in D3R (left) or D2R (right), poses from the last 2.4 ns of representative MD trajectories are shown. The side chains of the Ptm23 residues (Val86$^{2.61}$, Leu89$^{2.64}$, Gly94^{EL1}, Phe106$^{3.28}$, and Cys181^{EL2}) are shown in green sticks in **B-G**.

Figure 3. Receptor-ligand distances for D3R/R-22, D3R/C4, and D3R/C3. **A**) To compare the orientations of the bound ligands in Ptm23 in the MD simulations, distances (cyan dotted lines) were measured between the last carbon atom of the ligand linker region and the center of mass of the Cα atoms of three Ptm23 residues Val$^{2.61}$, Leu$^{2.64}$, and Phe$^{3.28}$ (the gray sphere labeled with "COM") (*a*), and between the center of mass of the SP indole ring moiety and the Cα atom of Gly94 (*b*). The receptor backbone is in gray ribbons, side chains of the Ptm23 residues are in green sticks, and R-22 is in orange sticks. **B**) A scatterplot of the receptor-ligand distances, *a* and *b*, from the last 2.4 ns of representative MD trajectories of D3R/R-22 (orange diamonds), D3R/C4 (yellow triangles), and D3R/C3 (magenta squares) shows that the SP moiety of the C3 analog is positioned farther away from the Ptm23 sub-pocket than those of R-22 and the C4 analog.

Figure 4. Conformational changes induced by R-22 and the C4 and C3 analogs in D3R. Side and top views (left and right panels, respectively) of the overlaid R-22-, C4-, or C3-bound D3R models (all in cyan) and the eticlopride-bound D3R model (gray) are shown. Conformational changes induced by R-22 (orange spheres in **A** and **B**) and C4 (yellow spheres in **C** and **D**) in D3R involve the extracellular segment of TM2 (C-terminal to Pro$^{2.59}$) shifting outward (orange arrows) relative to the eticlopride-bound model, resulting in a ~15° larger Prokink wobble angle. In contrast, for the C3 analog (magenta spheres in **E** and **F**) the Prokink angles do not differ significantly from the eticlopride-bound model.

Figure 5. Predicted hydration sites in the SBP of D3R (left) and D2R (right) bound to R-22 (orange, top) and C3 (magenta, bottom). High-energy hydration sites with a ΔG > 2.5 kcal/mol are also shown as large spheres (Beuming et al., 2009). Hydration sites that are in the Ptm23 sub-pocket (within 6 Å to the center of mass of Ptm23 residues Val$^{2.61}$, Leu$^{2.64}$, and Phe$^{3.28}$) are colored in red. Sites that are displaced by the ligand (within 2 Å of the indole group) are colored in blue, or have a blue silhouette if they are also in the Ptm23. Multiple high energy sites are displaced by the aryl amide in the R22-bound (orange) D3R model (**A**), but not in the C3 analog-bound D3R model (**C**), nor the R-22 bound (**B**) and the C3 analog-bound (**D**) D2R models.

Figure 6. The role of EL1 in determining R-22 binding affinity to D3R and D2R. **A**) NT-TM1-IL1, EL1, and EL2 of D2R, alone or in combination, were exchanged with that of D3R. **B**) Schematic of the HTRF-based binding assay. Receptors were fused with SNAP at their N-terminus, which covalently binds a terbium-based donor chromophore that FRETs with an DY-647-conjugated NAPS molecule bound to the OBS. **C**) D3R EL1, but not NT-TM1-IL1 or EL2, enhances R-22 binding affinity to D2R similarly to that at wild-type D3R. **D**) Addition of a single Gly residue after position 98 of D2R EL1 is sufficient to enhance R-22 affinity similarly to that at D3R. Deletion of Gly94 of D3R reduces R-22 affinity similarly to that at D2R. **E**) Mutation of

33

either D2R E99 or E181 to Val has no significant effect on R-22 binding affinity. Binding curves

are representatives of at least three independent experiments, for which data are summarized in

Table 2.

Figure 7. Comparison of the structural rearrangement in TM2 and EL1 induced by binding

of bulky ligands in β1- and β2-adrenergic receptors (β$_1$AR and β$_2$AR). **A**) Superposition of the

cyanopindolol-bound structure (PDB ID: 2VT4, cyanopindolol in dark gray, receptor in light gray)

and the carvedilol-bound structure (PDB ID: 4AMJ, carvedilol in blue, receptor in cyan) of β$_1$AR

shows an outward movement of the extracellular segment of TM2 in the presence of bulky

ligand carvedilol, resulting in a 2.3 Å shift of the Cα atom of Gly105 in EL1, and thereby an

outward tilting of the extracellular portion of TM2, compared to the cyanopindolol-bound

structure. **B**) Superposition of the ICI-118551-bound structure (PDB ID: 3NY8, ICI-118551 in

dark gray, receptor in light gray) and the FAUC50-bound structure (PDB ID: 3PDS, FAUC50 in

blue, receptor in cyan) of β$_2$AR shows similar conformations of TM2 and EL1 in the presence of

these two ligands. The structures were superimposed by the Cα atoms.

Table 1. Radioligand binding assay in D2R and D3R

	D2R		D3R		D2R/D3R
	pK$_i$	S.E.M.	pK$_i$	S.E.M.	
NAPS	9.47	0.04	9.26	0.06	0.6
R22[γ]	6.82	0.01	9.02	0.07	157.2
C3	7.07	0.04	7.31	0.06	1.7
C4[γ]	7.24	0.01	8.90	0.06	45.7
C5[γ]	7.48	0.09	8.42	0.06	8.8

Statistical significance was determined by one-way ANOVA with Bonferroni post hoc test.
[γ] indicates that the pK$_i$ at D2R and D3R for a given compound are significantly different ($p < 0.05$)

Table 2. HTRF whole cell binding affinities of NAPS and R-22 at chimera and mutant constructs

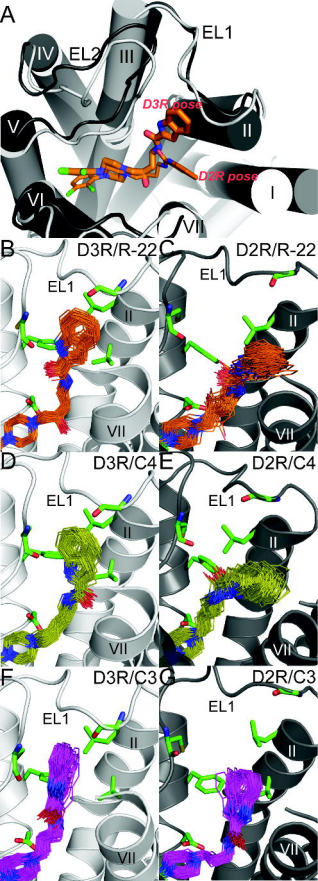| Construct	NAPS					R-22			
	pK$_i$	S.E.M.	Fold affinity increase (relative to D2R wildtype)	Fold affinity decrease (relative to D3R wildtype)		pK$_i$	S.E.M.	Fold affinity increase (relative to D2R wildtype)	Fold affinity decrease (relative to D3R wildtype)
D3R	9.21	0.14	1.2	1.0		8.37	0.13	48.0	1.0
D3R(Δ94G)	9.41	0.19		0.6		6.99$^\gamma$	0.23		24.1
D2R_D3R(EL1)	9.60	0.15	2.9			7.78$^\sigma$	0.02	12.4	
D2R_D3R(EL2)	9.21	0.12	1.2			6.41$^\sigma$	0.04	0.5	
D2R_D3R(EL1_EL2)	9.44	0.08	2.0			8.10$^\delta$	0.02	25.9	
D2R_D3R(NT-TM1-IL1)	9.51	0.10	2.4			6.62$^\gamma$	0.01	0.9	
D2R_D3R(NT-TM1-IL1_EL1)	9.47	0.15	2.2			7.83$^\sigma$	0.05	13.7	
D2R_D3R(NT-TM1-IL1_EL2)	9.28	0.08	1.4			6.57$^\gamma$	0.03	0.8	
D2R_D3R(NT-TM1-IL1_EL1_EL2)	9.04	0.08	0.8			7.89$^\delta$	0.01	15.9	
D2R(98-99GGV)	9.57	0.18	2.8			7.76$^\sigma$	0.00	11.7	
D2R(98-99GGE)	9.56	0.13	2.7			7.89$^\delta$	0.03	15.9	
D2R(E99V)	9.53	0.11	2.5			6.33$^\sigma$	0.02	0.4	
D2R(E181V)	9.49	0.17	2.3			6.28$^\sigma$	0.02	0.4	
D2R	9.13	0.24	1.0	1.2		6.69	0.08	1.0	48.0

Statistical significance was determined by one-way ANOVA with Bonferroni post hoc test.
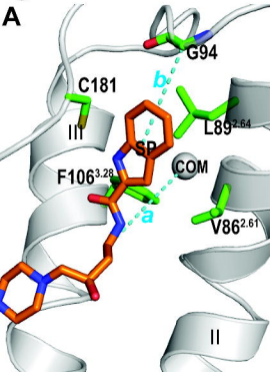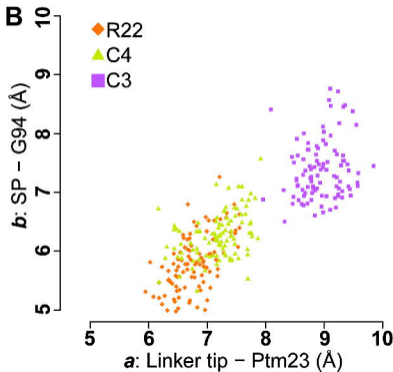
None of the mutations significantly altered the pK$_i$ values for NAPS ($p>0.1$).

For R-22, $^\gamma$ indicates that the pK$_i$ is significantly different from that at D3R ($p<0.001$) but not at D2R ($p>0.1$), $^\delta$ indicates that the pK$_i$ is significantly different from that at D2R ($p<0.001$) but not at D3R ($p>0.1$), whereas $^\sigma$ indicates that the pK$_i$ is significantly different from that at D2R ($p<0.001$) but also at D3R ($p<0.05$).
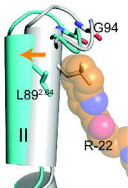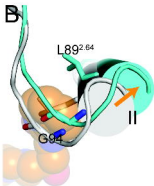
36

Figure 1

Figure 2

A

IV EL2 III EL1

V

D3R pose

II

D2R pose

VI I

VII

B D3R/R-22   C D2R/R-22

EL1   EL1

II   II

VII   VII

D D3R/C4   E D2R/C4

EL1   EL1

II   II

VII   VII

F D3R/C3   G D2R/C3

EL1   EL1

II   II

VII   VII

Figure 3

Figure 4

A — L89^2.64, II, G94, R-22

B — L89^2.64, G94, II

C — L89^2.64, II, G94, C4
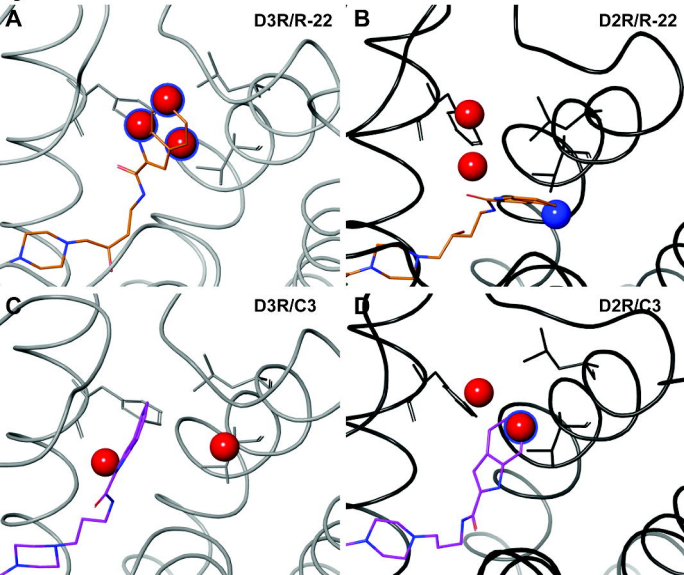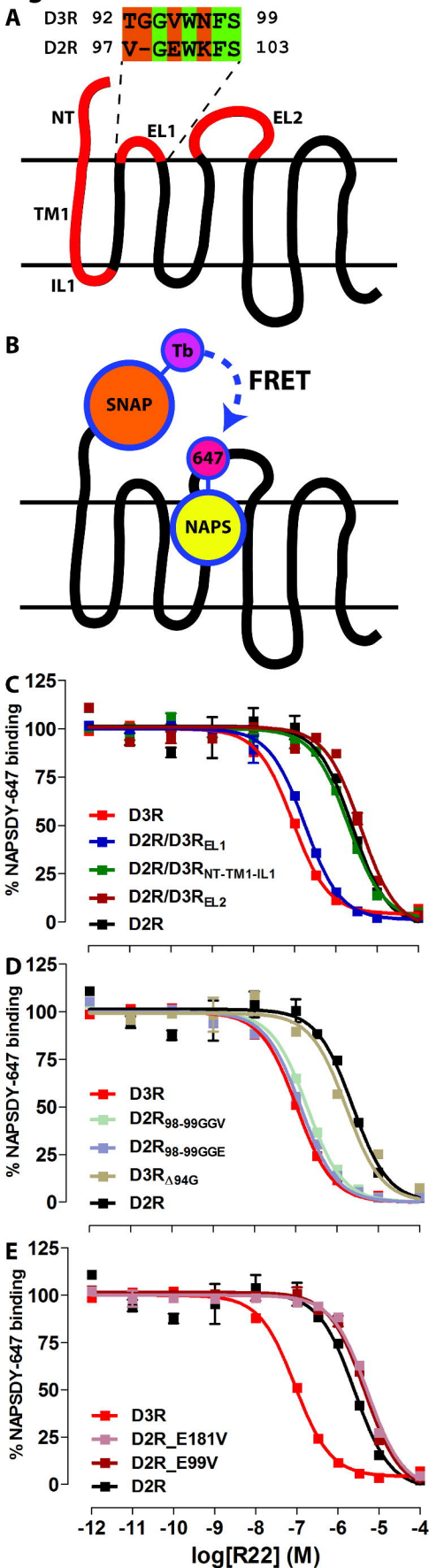
D — L89^2.64, G94, II

E — L89^2.64, II, G94, C3

F — L89^2.64, II, G94
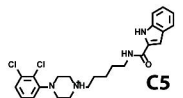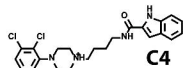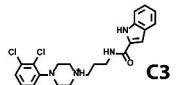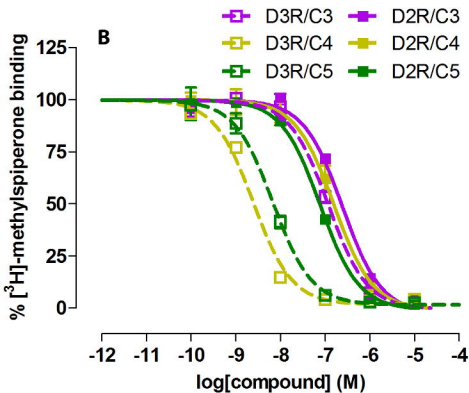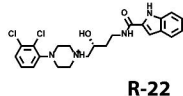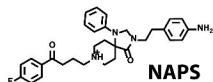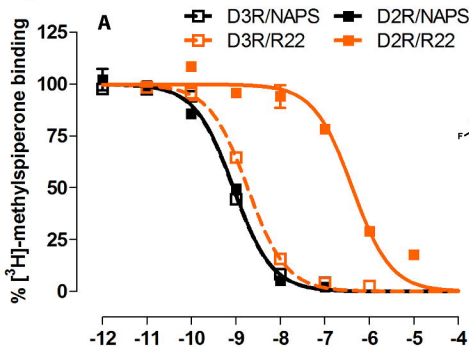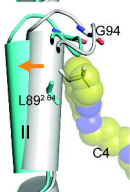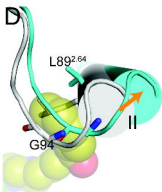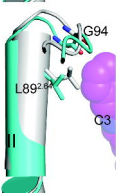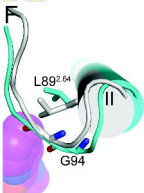
Figure 5

Figure 6

Figure 7